Evidence for aggregation-independent, PrP^C-mediated Aβ cellular internalization

Alejandro R. Foley[a,1], Graham P. Roseman[a,1], Ka Chan[a], Amanda Smart[a], Thomas S. Finn[a], Kevin Yang[a], R. Scott Lokey[a], Glenn L. Millhauser[a,2], and Jevgenij A. Raskatov[a,2]

[a]Department of Chemistry and Biochemistry, University of California, Santa Cruz, CA 95064

Edited by Samuel H. Gellman, University of Wisconsin–Madison, Madison, WI, and approved October 8, 2020 (received for review May 8, 2020)

Evidence linking amyloid beta (Aβ) cellular uptake and toxicity has burgeoned, and mechanisms underlying this association are subjects of active research. Two major, interconnected questions are whether Aβ uptake is aggregation-dependent and whether it is sequence-specific. We recently reported that the neuronal uptake of Aβ depends significantly on peptide chirality, suggesting that the process is predominantly receptor-mediated. Over the past decade, the cellular prion protein (PrP^C) has emerged as an important mediator of Aβ-induced toxicity and of neuronal Aβ internalization. Here, we report that the soluble, nonfibrillizing Aβ (1–30) peptide recapitulates full-length Aβ stereoselective cellular uptake, allowing us to decouple aggregation from cellular, receptor-mediated internalization. Moreover, we found that Aβ (1–30) uptake is also dependent on PrP^C expression. NMR-based molecular-level characterization identified the docking site on PrP^C that underlies the stereoselective binding of Aβ (1–30). Our findings therefore identify a specific sequence within Aβ that is responsible for the recognition of the peptide by PrP^C, as well as PrP^C-dependent cellular uptake. Further uptake stereodifferentiation in PrP^C-free cells points toward additional receptor-mediated interactions as likely contributors for Aβ cellular internalization. Taken together, our results highlight the potential of targeting cellular surface receptors to inhibit Aβ cellular uptake as an alternative route for future therapeutic development for Alzheimer's disease.

Alzheimer's disease | amyloid β | prion protein (PrP) | mirror-image peptides | receptor-mediated internalization

Amyloid β (Aβ) is an aggregation-prone peptide, typically ranging in length from 36 to 43 amino acids, released into the extracellular matrix by the proteolytic cleavage of the transmembrane amyloid precursor protein (APP) (1). Formation of amyloid plaques is a hallmark of Alzheimer's disease (AD); however, it is the soluble Aβ aggregation intermediates, often referred to as oligomers, that are the most neurotoxic species (2, 3). While Aβ degradation is facilitated by cellular uptake via glial cells (4), increasing evidence suggests that intracellular accumulation of Aβ may play an early role in AD pathogenesis (5–7), including mitochondrial dysfunction (8), synaptic impairment (7), and increased seeding and prion-like cellular propagation (9). Cellular uptake of soluble, nanomolar concentrations of Aβ leads to intracellular endosomal and lysosomal Aβ concentration, facilitating the formation of high-molecular-weight species capable of seeding amyloid fibril growth (10). This cell-uptake-induced aggregation has been shown to contribute to cellular death, ultimately leading to the release of amyloid species to the extracellular matrix (11). Thus, elucidating the mechanisms by which Aβ is internalized and accumulated inside the cells becomes critical to better understanding the early development of AD.

Various Aβ cellular internalization mechanisms have been reported, such as pore formation (3, 12), endocytosis (13), and receptor-mediated uptake (14). Over the past decade, numerous cell-surface receptors of Aβ have been proposed for the uptake of Aβ. These include the α7 nicotinic acetylcholine receptor (15) and the low-density lipoprotein receptor-related protein-1 (LRP1) (16, 17). Inhibition of soluble Aβ species interacting with the cell surface (18), membrane receptors (19), or blocking Aβ uptake (16) have been shown to reduce Aβ-induced toxicity. Over 400 clinical trials targeting Aβ aggregation have failed (20). In late 2019, the Aducanumab antibody that binds soluble Aβ aggregates showed some limited benefit in a phase III clinical trial (21), supporting the hypothesis that Aβ aggregation is important in AD. Targeting soluble, toxic forms of oligomeric Aβ remains the most promising avenue for AD therapeutic development, but it needs to be substantially improved to make real impact on lives of AD patients. Targeting interactions of Aβ with high-affinity receptors that lead to Aβ cellular internalization may offer a promising alternative for therapeutic development.

Using a cell-based screen of 225,000 clones from a mouse brain complementary DNA library, Strittmatter and coworkers found the cellular prion protein (PrP^C) binds to Aβ oligomers with the highest affinity as compared to the clones screened, displaying a dissociation constant less than 100 nM (22), leading to a PrP^C-dependent inhibition of long-term potentiation (LTP) in neurons (22) and memory impairment in AD mouse models (23). Subsequent work demonstrated that the PrP^C–Aβ interaction occurs in AD patients (24) and drives an aberrant signaling cascade mediated by mGluR5 (25, 26) leading to Fyn kinase phosphorylation in neurons. Additional research has demonstrated that PrP^C, in

Significance

Amyloid β (Aβ) aggregation has been the therapeutic target of several Alzheimer's disease (AD) clinical trials. Aβ exists in many different aggregated forms, making it exceedingly challenging to target. Evidence links intracellular Aβ accumulation and AD pathogenesis. We report that amino acids 1 to 30 of Aβ, Aβ (1–30), do not aggregate yet display cellular uptake stereospecificity when compared to its mirror image, suggesting that Aβ uptake is predominantly receptor-mediated and may be independent from its aggregation state. Additionally, we found Aβ (1–30) internalization to depend on PrP^C expression. Aβ (1–30) thus represents a powerful tool to study mechanisms of Aβ cellular internalization and suggests that Aβ uptake could be modulated by therapeutically targeting high-affinity Aβ receptors.

Author contributions: A.R.F., G.P.R., T.S.F., R.S.L., G.L.M., and J.A.R. designed research; A.R.F., G.P.R., K.C., A.S., and K.Y. performed research; A.R.F., G.P.R., K.C., A.S., K.Y., R.S.L., G.L.M., and J.A.R. contributed new reagents/analytic tools; A.R.F., G.P.R., K.C., A.S., T.S.F., K.Y., R.S.L., G.L.M., and J.A.R. analyzed data; and A.R.F., G.P.R., G.L.M., and J.A.R. wrote the paper.

The authors declare no competing interest.

This article is a PNAS Direct Submission.

[1]A.R.F. and G.P.R. contributed equally to this work.

[2]To whom correspondence may be addressed. Email: glennm@ucsc.edu or jraskato@ucsc.edu.

This article contains supporting information online at https://www.pnas.org/lookup/suppl/doi:10.1073/pnas.2009238117/-/DCSupplemental.

First published November 2, 2020.

conjunction with LRP1, facilitates cellular uptake of Aβ (16), causing an increase in Fyn kinase phosphorylation.

In previous experiments we compared toxicity of L- and D-Aβ42. We found that, under conditions where L-Aβ42 reduced cell viability over 50%, D-Aβ42 was either nontoxic (PC12) or under 20% toxic (SH-SY5Y) (27). We later showed that L-Aβ is taken up approximately fivefold more efficiently than D-Aβ (28), suggesting that neuronal Aβ uptake and toxicity are linked. Here, we used the mirror-image strategy to pinpoint specific sites within Aβ that are responsible for this stereodifferentiation. Furthermore, we used PrP^C-transfected cells as a high-affinity receptor of Aβ to showcase the relevance of receptor-mediated mechanisms leading to cellular internalization.

Results

We first examined how PrP^C expression influenced Aβ uptake in HEK293T cells, which do not naturally express PrP^C (29). We chose the Aβ40 system for its lower propensity to form pores in cellular membranes (30) and lipid bilayers (12), therefore making it suitable to study receptor-mediated interactions. We synthesized Aβ peptides by solid-phase peptide chemistry, yielding purities exceeding 96% (*SI Appendix*, Figs. S1–S5). For uptake studies, we N-terminally labeled Aβ (1–40) peptides with 5(6)-carboxytetramethylrhodamine (TAMRA), which we have shown previously does not change Aβ aggregation and toxicity (28). As quantitated by flow cytometry (Fig. 1 *B* and *C*), there is a 3.8-fold difference between L- and D-Aβ. When PrP^C is transfected and expressed, both L-Aβ40 and D-Aβ40 values increase (fourfold and 2.2-fold, respectively), and the difference between L-Aβ40 and D-Aβ40 rises to 7.3-fold. Transfection buffer had no effect on cellular association (*SI Appendix*, Fig. S7*A*) and increased PrP^C expression levels result in a dose-dependent behavior (*SI Appendix*, Fig. S7*B*). Z stacks obtained from confocal imaging reveal that Aβ40 peptides are mostly internalized rather than bound to the cellular membrane (Fig. 1 *D*–*G*), qualitatively showing an increase in cellular uptake for L-Aβ40 compared to D-Aβ40 (green color indicated with arrows) (Fig. 1 *D* and *F*). Furthermore, PrP^C-expressing HEK293T cells display an increase in internalized TAMRA-L-Aβ40 (Fig. 1 *E* and *G*) relative to untransfected cells, which is consistent with the flow cytometry results. While L-Aβ40 uptake increases fourfold upon PrP^C expression, D-Aβ40 uptake also increases (2.2-fold), suggesting that both stereospecific and nonspecific interactions between PrP^C–Aβ40 might be involved in increased Aβ uptake, with stereospecific interactions contributing at a higher degree. Additionally, Aβ40 uptake is reduced for PrP^C constructs that delete (ΔCR and Δ100–109 PrP^C) or mutate (G5 PrP^C) the putative binding site of Aβ on wild-type (WT) PrP^C (*SI Appendix*, Fig. S8) (22). Intriguingly, QCR PrP^C, which mutates four conserved lysines between residues 100 and 109 known to influence a PrP^C–Aβ interaction (31) to glutamines, does not result in a decrease in uptake.

Enantiomeric peptides are usually employed to differentiate receptor-mediated from achiral-based toxicity and uptake mechanisms, such as pore formation or passive permeability (32). However, recent work performed by Craik and coworkers demonstrated that the chirality of membrane phospholipids can also modulate interactions of peptides with membranes (33). To address this effect, we performed liposome association controls in lipid unilamellar vesicles composed of 99% phosphatidylcholine (PC) (achiral headgroups) and 1% brain-derived phosphatidylserine (PS) (chiral headgroups). Our results show that both TAMRA-L-Aβ40 and TAMRA-D-Aβ40 associate to liposomes at similar levels, establishing that the observed stereoselectivity of cellular uptake of Aβ is not due to chiral interactions with the lipid bilayer itself (*SI Appendix*, Fig. S9).

We then sought to investigate sequences within Aβ responsible for these stereospecific interactions. Thus, we synthesized truncated variants of Aβ including the flexible N-terminal region

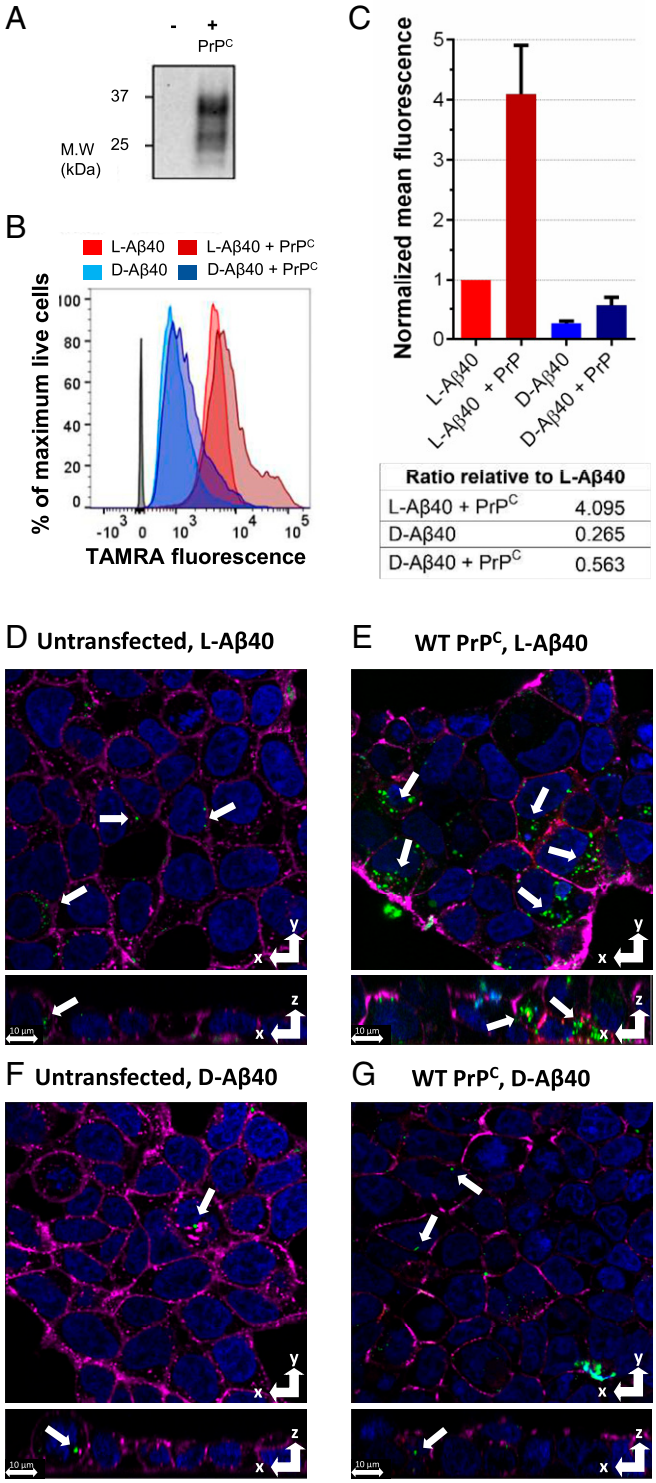

Fig. 1. Aβ40 uptake in HEK293T cells (5 μM peptide, 2-h incubation). (*A*) Western blot showing PrP^C expression. (*B*) Representative FACS diagram. (*C*) Mean FACS quantitation, with error bars showing SD from three biological replicates, and table below showing relative ratios. (*D*–*G*) Representative confocal images from Z stacks. Magenta: membrane dye; green: TAMRA-Aβ; red: PrP^C dye; blue: nuclear dye. (*D*) L-Aβ40 (no PrP^C). (*E*) L-Aβ40 + PrP^C. (*F*) D-Aβ40 (no PrP^C). (*G*) D-Aβ40 + PrP^C. White arrows mark TAMRA-Aβ peptides. (Scale bars, 10 μm.)

(Fig. 2*A*), which we hypothesized to be more available for intermolecular interactions given its greater flexibility when compared to the hydrophobic C terminus of Aβ (34). We observed in SH-SY5Y cells that Aβ (1–16) sequence retained little stereoselectivity (1.4-fold of L over D). In contrast, substantial stereodifferentiation arose with amino acids 16 to 30, where Aβ (16–30) and Aβ (1–30) sequence showed a 4.2-fold and 4.3-fold L vs. D difference, respectively (Fig. 2*B*). These differences are comparable to full-length Aβ40. We then tested these sequences in PrP^C-transfected HEK293T cells (Fig. 2*C*). While stereodifferentiation for the different Aβ fragments in untrasfected cells followed the same trend as in SH-SY5Y cells, surprisingly we did not observe a PrP^C-dependent uptake for Aβ (16–30). However, L-Aβ (1–30) showed a PrP^C-dependent increase in uptake, with trends similar to full-length L-Aβ40. Importantly, the Aβ (1–30) segment is soluble, does not aggregate, and retains a random-coil conformation for at least 24 h (*SI Appendix*, Figs. S10 and S11), which is consistent with previous studies on the Aβ (1–28) system (35). These properties of Aβ (1–30) pointed to the existence of a specific site, responsible, at least in part, for Aβ interactions with PrP^C, as well as its cellular internalization.

Since the nonaggregating Aβ (1–30) was sufficient to recapitulate the trends in PrP^C-dependent uptake stereoselectivity, we studied its interaction with PrP^C using NMR. We collected ^1H-^{15}N heteronuclear single quantum coherence (HSQC) spectra on uniformly ^{15}N-labeled PrP^C with or without L- or D-Aβ (1–30). Intensity ratios (I/I_o) and weighted averaged chemical shifts (Δ) were calculated for each assigned amino acid (data in *SI Appendix*, Tables S1 and S2) and then plotted as bar graphs (Fig. 3). For D-Aβ (1–30), we observed minimal changes in I/I_o throughout the assigned amino acids, indicating little interaction. In contrast, L-Aβ (1–30) displayed a decrease in I/I_o values for assigned amino acids between residues 94 and 125, with the largest decrease between residues 94 and 110. This region also displayed small changes in Δ, indicating an overall intermediate exchange, or moderate affinity for the PrP^C-L-Aβ (1–30) interaction (36). There is additional change in chemical shifts for the structured C terminus [N-terminal side of Helix 1 (H1) and N-terminal end of Helix 2 (H2)] for both L- and D-Aβ (1–30); however, the Δs are not accompanied by appreciable decreases in I/I_o, indicating a fast exchange regime and perhaps nonspecific interactions. Overall, these results correlate with other studies showing oligomeric Aβ (1–42) binds to residues 94 to 110 on PrP^C (22, 37). Furthermore, our NMR results are consistent with our cell studies demonstrating a decrease in uptake when this region is deleted or mutated from full-length WT PrP^C (*SI Appendix*, Fig. S8).

Discussion

Previous studies have shown that PrP^C preferentially interacts with oligomeric Aβ over nonaggregated Aβ (22, 38). In contrast, we have shown that nonaggregating Aβ (1–30) can interact with PrP^C and lead to increased cellular uptake. Importantly, soluble L-Aβ (1–30) interacts with PrP^C between residues 94 and 110, which is the known docking site of oligomeric Aβ (22, 37), thus demonstrating that the absence of Aβ residues 31 to 40 does not affect the locus of binding to PrP^C. We also observed higher PrP^C-dependent uptake of the natural L-isoforms of both Aβ (1–30) and Aβ40 when compared to the D-enantiomers, suggesting a docking site on PrP^C facilitating this interaction.

It has been proposed that an Aβ binding partner relevant to synaptic dysfunction in AD will be 1) oligomer-specific, 2) high-affinity, and 3) present in adult synapses (39). Previous studies have demonstrated that PrP^C contains these three characteristics (16, 22, 25, 26, 38–40). However, our results demonstrate that PrP^C can bind to Aβ (1–30), which is highly soluble, does not aggregate, and remains stable as a single species with a random-coil conformation. This conceivably points to Aβ (1–30)'s not being a higher-order oligomer while still retaining stereoselective uptake and PrP^C binding. This implies that Aβ (1–30) may be the amino acid sequence within full-length Aβ that allows for a PrP^C–Aβ interaction, whereas residues 31 to 40 in full-length Aβ could have a major and main role in promoting Aβ oligomerization. Furthermore, oligomerization could potentially enrich for the preferred conformation of Aβ (1–30) that facilitates an interaction with PrP^C, which is in agreement with our results showing higher PrP^C-dependent cellular uptake levels of Aβ40 when compared to Aβ (1–30) (Fig. 2). This is supported by recent evidence showing that different oligomeric Aβ conformations, measured by accessibility of conformational antibodies, bind with different affinities to PrP^C (41).

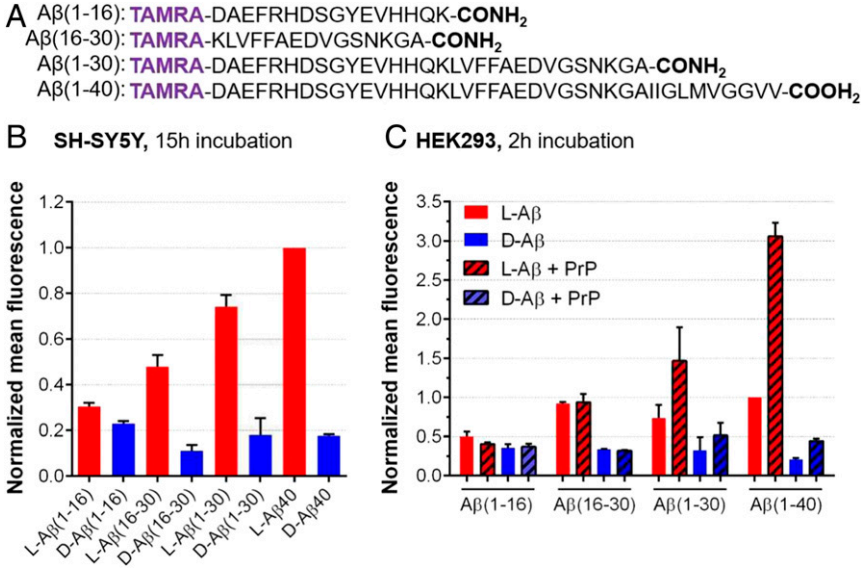

Fig. 2. Cellular uptake of the Aβ peptides studied in this work. (*A*) Sequence of Aβ peptides tested. (*B*) Mean FACS results in SH-SY5Y cells normalized against L-Aβ40 (5 μM peptide, 15-h incubation). Bars show mean fluorescence with error bars for SD of three biological replicates. (*C*) Mean FACS results in HEK293T cells with and without PrP^C expression, normalized against L-Aβ40 (5 μM peptide, 2-h incubation). Bars show mean fluorescence with error bars for SD of two biological replicates.

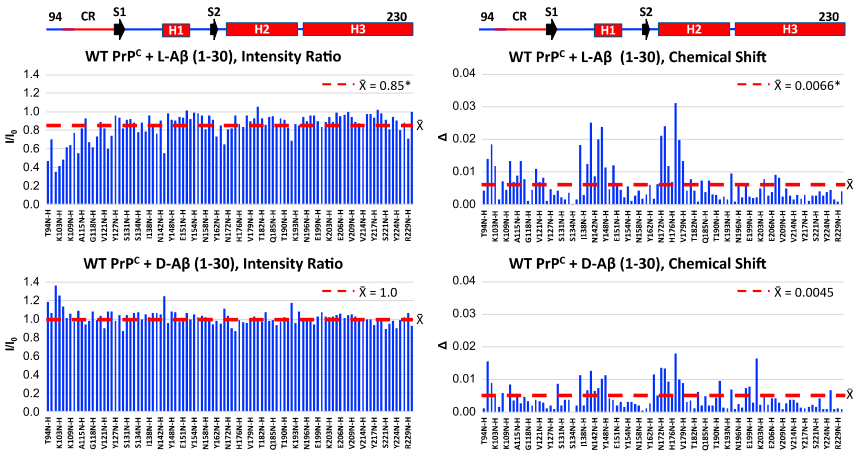

Fig. 3. Effect of 200 μM L-Aβ (1–30) or D-Aβ (1–30) on the intensities ratios (I/I_o) or chemical shifts (Δ) of 100 μM WT-PrP^C resonances recorded in a ^{1}H- ^{15}N HSQC spectrum at room temperature in 10 mM MES (pH 6.6). Linear schematics above line up with bar graphs. CR: central region (amino acids 105 to 125). The red lines on the intensity ratio and chemical shift graphs are centered at the average value ($\bar{X}$) for the respective data set. The asterisk (*) next to the $\bar{X}$ values denotes a statistically significant difference when comparing the $\bar{X}$ values for the intensity ratios or chemical shifts induced by either L-Aβ (1–30) or D-Aβ (1–30) using the nonparametric Wilcoxon matched- pairs signed rank test ($P < 0.0001$), as appropriate for non-Gaussian distributions.

Mounting evidence shows physiological relevance to a PrP^C–Aβ interaction. For example, monoclonal antibodies directed to target PrPC–Aβ binding sites protected against the Aβ-mediated block of LTP in C57BL/6J mice in vitro and in vivo (42). However, other studies have exhibited PrP^C-independent neurotoxicity in AD models (43, 44). From our results, we observed a PrP^C-independent, but still stereoselective, uptake of L-Aβ (16–30). While PrP^C–Aβ binding seems to require amino acids (1–30), the (16–30) sequence may be sufficient for other chiral interactions with cells, and resolving these chiral interactions may reveal novel receptors as targets to develop therapeutics to inhibit Aβ cellular uptake beyond PrP^C. For example, Aβ oligomers have been shown to bind to the neuronal cell surface receptor LilrB2, producing deleterious effects on hippocampal LTP in mice, resulting from impaired neuronal signaling and thus generating synaptotoxicity (45). Further studies of Aβ–LilrBr2 interactions led to the identification of Aβ moiety 16–21 (^{16}KLVFFA^{21}) as responsible for the interaction with LilrBr2, and small molecules designed to block this interaction were shown to reduce Aβ toxicity in in vitro models (19). Additionally, the tyrosine kinase EphB2 receptor, which modulates the activity of *N*-methyl-D-aspartate–type glutamate receptors, has been reported to interact with Aβ oligomers (46), and blocking this interaction with small peptides results in the rescue of impaired synaptic plasticity and memory deficits in AD APPswe/PS1dE9 (APP/PS1) transgenic mice (47). Other receptors linked in AD pathogenesis include α7 nicotinic acetylcholine receptor (15) or LRP1 (16, 17).

While receptor-mediated interactions of Aβ can lead to downstream neurotoxicity, there are additional mechanisms by which Aβ–membrane interactions may be deleterious. Lipid membranes themselves are known to bind Aβ by either the phospholipid head groups (48) or through the interaction of additional membrane components such as cholesterol, the later reported to catalyze Aβ aggregation in synthetic lipid membranes (49). Cellular plasma membranes also promote Aβ self-assembly, aggregation, and internalization, in a process that generates cytotoxic Aβ species (50). In contrast, Aβ (1–30) does not aggregate, yet we showed it can participate in cell-surface interactions that lead to stereoselective cellular uptake. An increase in intracellular Aβ can create local gradients of particularly high concentrations of Aβ which may favor intracellular Aβ aggregation, ultimately leading to increased pathogenicity and extracellular release of Aβ aggregates which can further act as a seed for fibril growth (10, 11). Abnormally high concentrations of intracellular Aβ resulting from Aβ uptake can also result in decreased Aβ solubility, promoting a homeostatic intracellular imbalance that could trigger amyloid formation (51). Factors controlling Aβ trafficking into cells are therefore of seminal importance to prevent AD pathogenesis (52), and modulating receptor-mediated Aβ uptake could represent a promising strategy for AD disease prevention. In addition, sporadic AD and resulting dementia may be associated with infections of brain tissue with pathogens that are known to enter into neurons, such as herpes simplex virus 1 (HSV-1) and porphyromonas gingivalis (53, 54). As a result, those HSV-1–infected cells produce more Aβ (55), a mechanism that has recently been exploited for the development of brain-tissue models of AD (56).

Taken together, we found that the soluble, nonfibrillizing Aβ (1–30) peptide recapitulates uptake stereoselectivity of full-length Aβ (28). Our findings show that molecular cell-surface recognition of Aβ underlying its internalization is largely due to the amino acid sequence and not the state of aggregation. We found that the soluble Aβ (1–30) peptide segment is both necessary and sufficient to recapitulate stereospecific and PrP^C-dependent uptake. Solution NMR demonstrated that L-Aβ (1–30) interacts with WT-PrP^C between residues 94 and 110, in agreement with previous studies (22, 37), thus validating L-Aβ (1–30) as model system to study this disease-relevant interaction. Deletion of this PrP^C site resulted in a decrease in PrP^C-dependent uptake of Aβ40, further demonstrating a functional interaction between PrP^C and the (1–30) segment of Aβ. These results are consistent with a model in which the relatively flexible segment (1–30) is responsible for cell-surface recognition, whereas the hydrophobic C terminus orchestrates Aβ aggregation and may act in membrane docking and/or perforation activity (12, 30). Future efforts targeting this specific sequence, as well as its cellular binding partners, may hold therapeutic potential to inhibit Aβ toxicity.

Materials and Methods

Synthesis of Aβ Peptides. Aβ and derived peptides were synthesized by solid-phase chemistry, following our previously reported protocols (27). L-Aβ40 and D-Aβ40 were synthesized using Tentagel PHB resin (Rapp Polymere) to achieve carboxyl C terminus, while Aβ fragments were synthesized using Rink Amide resin (Creosalus) to yield amidated C terminus. All syntheses were performed on a CEM Liberty Blue automated microwave-assisted peptide synthesizer at 0.1 mM scale relative to resin loading. Thirty percent

piperidine (Spectrum) in dimethylformamide (DMF) was used for deprotection steps, and 1-hydroxybenzotriazole hydrate (Oakwood Chemical) and *N*,*N*′-diisopropylcarbodiimide (Chem-Impex) were used as coupling reagents. Peptides were cleaved and deprotected with a mixture solution consisting of trifluoroacetic acid (10 mL), 1, 2-diethanethiol (0.5 mL), tri-isopropylsilane (1 mL), and liquefied phenol (0.5 mL). Peptides were purified by reverse-phase high-performance liquid chromatography (HPLC) as previously described (27), yielding peptides with purities exceeding 97% (*SI Appendix*, Figs. S3 and S4).

N-Terminal TAMRA Labeling of Aβ Peptides. One hundred milligrams of resin (1 eq.) with deprotected N terminus Aβ40 and derived peptides resin were swelled in 2 mL of DMF. Then, a mixture of TAMRA (10 eq.), benzotriazol-1-yl-oxytripyrrolidinophosphonium hexafluorophosphate (PyBOP, 10 eq.), 1-hydroxy-7-azabenzotriazole (HOAt, 16 mg, 20 eq.), and diisopropylethylamine (10 eq.), was dissolved in 5 mL of DMF and added to the resin. The TAMRA–resin mixture was agitated on a rotational shaker for 24 h protected from light. The resin was then washed with DMF (three times) and DCM (two times) and vacuum-dried for 30 min. Reaction completion was confirmed by a cleavage and mass spectrometry analysis of a small fraction of reacted resin. Purification of the peptides was performed as described above, yielding peptides with purity exceeding 96% (*SI Appendix*, Figs. S3–S5). TAMRA $\lambda_{ex/em}$ was 550/580 nm.

Cellular Cultures.

SH-SY5Y cells. Human neuroblastoma SH-SY5Y cells (ATCC) were cultured in 1:1 Dulbecco's Modified Eagle's Medium (DMEM):F12 K media supplemented with 10% fetal bovine serum and 1% penicillin–streptomycin.

SH-SY5Y cell preparation for flow cytometry experiments. Cells were seeded into six-well plates at a density of 5×10^4 cells per well (2 mL) and allowed to adhere for 24 h before performing experiments.

HEK 293T cells. Human embryonic kidney HEK293T cells (ATCC) were cultured in high-glucose DMEM supplemented with 10% fetal bovine serum (Life Technologies) and GlutaMAX (Gibco).

HEK293T cell preparation for flow cytometry, Western blotting, and confocal microscopy experiments. Cells were first seeded into six-well plates at a density of 4×10^5 cells per well, where cells for confocal microscopy were first seeded into eight-well chamber slides (ibidi) at a density of 8×10^4 cells per well. Twenty-four hours after plating, the cells were transiently transfected using LipoD293 In Vitro DNA Transfection Reagent (SignaGEN Laboratories) with 1 μg (for fluorescence-activated cell sorting [FACS] experiments) or 0.25 μg (for confocal microscopy) of PrP^C encoding pcDNA3.1(+)Hygro plasmids. The media was changed 24 h after transfection with fresh DMEM and incubated overnight before starting dosing experiments.

Protein Expression. Recombinant PrP^C was prepared using previously established methods (57). In brief, recombinant PrP^C constructs encoding the various mouse PrP^C(23–230) constructs in the pJ414 vector (DNA 2.0) were transformed into and expressed using *Escherichia coli* (BL21 [DE3]; Invitrogen) (58).

Bacteria were grown in M9 minimal media supplemented with $^{15}NH_4Cl$ (1 g/L) (Cambridge Isotopes) for ^1H-^{15}N HSQC experiments or in Luria broth media (Research Product International). Cells were grown at 37 °C until reaching an optical density of 1 to 1.2, at which point expression was induced with 1 mM isopropyl-1-thio-D-galactopyranoside. PrP^C constructs were purified as previously described (59). Briefly, proteins were extracted from inclusion bodies with extraction buffer (8 M guanidium chloride (GdnHCl), 100 mM Tris, and 100 mM sodium acetate, pH 8) at room temperature and were purified by Ni^{2+}-immobilized metal-ion chromatography (IMAC). Proteins were eluted from the IMAC column using elution butter (5 M GdnHCl, 100 mM Tris, and 100 mM sodium acetate, pH 4.5) and were brought to pH 8 with 6 M potassium hydroxide (KOH) and left at 4 °C for 2 d to oxidize the native disulfide bond. Proteins were then desalted into 50 mM potassium acetate buffer (pH 4.5) and purified by reverse-phase HPLC on a C_4 column (Grace). Pure protein was lyophilized and stored at −20 °C until needed. The purity and identity of all constructs were verified by analytical HPLC and electrospray ionization mass spectrometry (ESI-MS). Disulfide oxidation was confirmed by reaction with *N*-ethylmaleimide and subsequent ESI-MS analysis.

Western Blotting Experiments. Whole-cell lysates were prepared by washing cells two times with phosphate-buffered saline (PBS). Cells were then lysed with lysis buffer [50 mM Tris(hydroxymethyl)aminomethane (Tris) (pH 8), 150 mM sodium chloride (NaCl), 1 mM ethylenediaminetetraacetic acid (EDTA), 1% Triton X-100, and 10% glycerol] supplemented with Halt Protease Inhibitor Mixture (Thermo Fisher Scientific) and quantified using Pierce BCA Protein Assay Kit (Thermo Fisher Scientific). To remove N-linked glycans, cell lysates were treated with recombinant PNGase F (New England Biolabs) under denaturing conditions according to the manufacturer's protocol. Completed PNGaseF reactions were boiled in sodium dodecyl sulfate polyacrylamide gel electrophoresis (SDS-PAGE) buffer and run on a 4 to 20% Mini-PROTEAN TGX Precast Protein Gels (Bio-Rad) along with Precision Plus Protein WesternC Blotting Standards (Bio-Rad). SDS-PAGE gels were subsequently washed with water three times totaling 15 min and transferred to a nitrocellulose membrane using Trans-Blot Turbo Transfer System (Bio-Rad). Membranes were blocked using 5% bovine serum albumin (BSA) in TBS-T. PrP^C constructs were probed with PrP^C Antibody (M-20) (sc-7694, goat origin; Santa Cruz Biotechnology) whose epitope matches near the C terminus of PrP^C. The PrP^C antibody was then detected with horseradish peroxidase (HRP) rabbit anti-goat immunoglobulin G (ab6741; Abcam) and the ladder was detected with Precision Protein StrepTactin-HRP Conjugate (Bio-Rad). Blots were exposed to Pierce ECL Western Blotting Substrate (Thermo Fisher Scientific) and images were taken using ChemiDoc XRS+ System (Bio-Rad) and analyzed using Image Lab Software (Bio-Rad).

Flow Cytometry Experiments. Flow cytometry experiments were performed as previously described (28). Briefly, lyophilized TAMRA-labeled peptides were dissolved in 20 mM NaOH and diluted to a final concentration of 5 μM using SH-SY5Y cell media. Original seeding media was removed from cells and replaced with the freshly prepared 5 μM TAMRA-labeled peptide solution. For control cells, original seeding media was replaced by fresh cell media with no peptide. Cells were then incubated for the desired amount of time at 37 °C. Following incubation time, cells were washed twice with 1× PBS, pH 7.4, trypsinized for 5 min, resuspended in cell culture media, centrifuged at $120 \times g$ for 10 min, resuspended in 1× PBS, pH 7.4, centrifuged at $120 \times g$ for 10 min, and then incubated for 20 min with 1× PBS, pH 7.4, containing 0.1% live/dead fixable violet dye (Thermo Fisher Scientific). Cells were then centrifuged and resuspended in FACS buffer solution (5 mM EDTA and 0.5% BSA in 1× Dulbecco's PBS [DPBS]). A population of 1×10^4 cells was analyzed on a BD FACS Aria II flow cytometer. Live/dead cell dye was excited at 405 nm and fluorescence was detected through a 450/30 nm filter. TAMRA was excited at 571 nm and fluorescence was detected through a 580/10-nm filter. Collected data were processed and analyzed using FlowJo software.

Confocal Microscopy Experiments. HEK293T cells were plated in an eight-well chamber slide (ibidi) as described in *Cellular Cultures*. Cells were dosed with TAMRA-Aβ peptides at 5 μM concentration, following the same sample reconstitution procedures as detailed for FACS. Cells were incubated for 2 h at 37 °C. After incubation, cells were washed twice with 1× DPBS (HyClone) and incubated for 20 min with a solution containing 5 μg/mL Hoechst 33342 dye (nuclear stain, $\lambda_{ex/em}$ 350/461 nm; ThermoFisher), 5 μg/mL wheat germ agglutinin Alexa Fluor dye (membrane stain, $\lambda_{ex/em}$ 650/668 nm; ThermoFisher), and 5 μg/mL PrP^C(8B4) Alexa Fluor dye (PrP^C-specific stain, $\lambda_{ex/em}$ 490/525 nm; Santa Cruz Biotechnology) in DPBS. After incubation, dye-containing solution was removed and cells were washed twice with 1× DPBS and resuspended again in 1× DPBS. Confocal images were acquired on a Leica SP5 confocal microscope using a 63×/1.4 to 0.6 oil immersion objective. Z stacks were collected by three sequential scans (PrP^C-Alexa Fluor & wheat germ agglutinin Alexa Fluor/TAMRA/Hoechst 33342) to avoid spectral overlapping. Images were analyzed using Imaris software.

NMR Experiments. Lyophilized uniformly ^{15}N-labeled PrP^C constructs were first suspended in water until fully solubilized and concentrations were checked using the absorbance at 280 nm (A_{280}) with the proper extinction coefficient. L- or D- Aβ (1–30) was first dissolved to 4 mM in 20 mM potassium hydroxide (KOH) and sonicated for 30 s in a bath sonicator until fully solubilized. The Aβ (1–30) solution was then subsequently diluted to 400 μM with 10 mM 2-(*N*-morpholino)ethanesulfonic acid (MES) at pH 6. NMR samples were contained 100 μM WT PrP^C with or without 200 μM L- or D-Aβ (1–30) in 10 mM MES buffer with 10% D_2O and the pH was adjusted to 6.6 using 600 mM KOH. Samples were loaded into a Shigemi NMR tube (BMS-005B; Wilmad Glass) and a ^1H- ^{15}N HSQC spectrum was collected at 25 °C on an 800-MHz spectrometer (Bruker) at the University of California, Santa Cruz NMR Facility. NMR spectra were analyzed with NMRPipe (60) and Sparky. Protein assignments were achieved using previously determined values (58). Intensity ratios (I/I_o) were calculated by dividing the peak intensity with Aβ (1–30) (I) by the peak intensity of WT PrP^C alone (I_o). The weighted average chemical shifts (Δ) were calculated by the equation $\Delta = [\Delta\delta_{HN}^2 + (0.17\ \Delta\delta_N^2)]^{1/2}$, where $\Delta\delta_{HN}$ and $\Delta\delta_N$ are the Aβ (1–30)–induced differences amide proton and nitrogen chemical shifts, respectively.

Synthetic Liposomes Experiments. A solution of 10 mg/mL 99:1 L-α-phosphatidylcholine (PC):L-α-phosphatidylserine (PS)-brain (Avanti Polar Lipids) in

DCM was blown down with N_2 to create a lipid film, which was then covered with a wipe and vacuum-desiccated for 3 h. The film was then rehydrated with 1× PBS, pH 7.4, and the liposome solution was rotated for 30 min. After mixing, unilamellar vesicles were extruded on a mini extruder with a 0.2-μm polycarbonate membrane over a heating block. The liposome crude solution was passed through the membrane a minimum of 40 times.

Dynamic light scattering characterization. Extruded liposomes diameter was measured on a Malvern Zetasizer Nano ZS90 particle analyzer using 1-cm path length cuvettes, with five runs of 10 s of run duration per run. Three measurements were taken per run with 0-s delay between measurements.

Incubation of liposomes with L-Aβ40-TAMRA and D-Aβ40-TAMRA. Confirmed-diameter liposomes were incubated in the dark for 2 h at room temperature with a 5 μM solution of either L-Aβ40-TAMRA or D-Aβ40-TAMRA in 1× PBS, pH 7.4. Association of TAMRA-Aβ samples to liposomes was determined by flow cytometry on a FACS Aria II flow cytometer, with excitation at 571 nm and fluorescence detection through a 580/10-nm filter. Liposomes incubated with 1× PBS, pH 7.4, only were used as a control.

TAMRA Quenching Kinetic Assays. Lyophilized Aβ peptides were dissolved in 20 mM NaOH, sonicated for 30 s, and diluted with 20 mM phosphate buffer, pH 7.4. Concentration was determined by Nanodrop (ε = 99,000 $M^{-1}{\cdot}cm^{-1}$) at 555 nm. As soon as samples were dissolved to the desired concentration, 200 μL were added to each well in a clear-bottom, black 96-well plate (Corning). Samples were monitored in a Biotek synergy HTX fluorescence plate reader (λ_{ex} = 550 nm, λ_{em} = 580 nm) at 37 °C with continuous shaking. All experiments were run in triplicate and the plate was sealed with optically clear adhesive film. Readings were collected every 5 min with 5 s of shaking before reading and 295 s of shaking in between readings.

Circular Dichroism Spectroscopy Experiments. Aβ (1–30) peptides were dissolved to 200 μM concentration (same as for NMR experiments) in 20 mM phosphate buffer (pH 7.4). To obtain the circular dichroism (CD) spectra, 400 μL of peptide-containing solution were placed in a quartz 1-mm cell. Spectra were then recorded using a Jasco 1500 CD spectrophotometer, set to a scan range of 180 to 280 nm, a digital integration time of 4 s, and a scan speed of 50 nm/min. Samples were incubated at 37 °C in between measurements.

Size-Exclusion Chromatography Experiments. Aβ (1–30) lyophilized peptides were reconstituted to 200 μM in 20 mM phosphate buffer, pH 7.4, as previously described. The solution was injected to a Yarra SEC-2000 column at 0.6 mL/min flow rate on a 1260 Agilent Infinity II LC system, using 20 mM phosphate buffer, pH 7.4, as running buffer. Absorbance at 214 nm was used as method of detection. Peptides were incubated at 37 °C for time = 24-h measurements.

Data Availability. All study data are included in the paper and *SI Appendix*.

ACKNOWLEDGMENTS. J.A.R. thanks University of California, Santa Cruz (UCSC) for start-up funds. We thank NIH for funding: J.A.R. (R21AG058074), A.R.F. (2R25GM058903-20-IMSD), G.L.M. (R35GM131781, S10OD024980, and S10OD018455), and R.S.L and K.Y. (GM131135). We thank Prof. M. Vendruscolo, Prof. D. Kliger, and Dr. E. Chen for helpful comments, UCSC NMR facility, and UCSC microscopy facility and Dr. Benjamin Abrams for help with confocal imaging and critical discussions. We thank B. Nazario for the help with flow cytometry experiments and Phenomenex for the generous donation of a size-exclusion chromatography column.

1. R. J. O'Brien, P. C. Wong, Amyloid precursor protein processing and Alzheimer's disease. *Annu. Rev. Neurosci.* **34**, 185–204 (2011).
2. C. Haass, D. J. Selkoe, Soluble protein oligomers in neurodegeneration: Lessons from the Alzheimer's amyloid beta-peptide. *Nat. Rev. Mol. Cell Biol.* **8**, 101–112 (2007).
3. R. Kayed *et al*., Common structure of soluble amyloid oligomers implies common mechanism of pathogenesis. *Science* **300**, 486–489 (2003).
4. M. Ries, M. Sastre, Mechanisms of Aβ clearance and degradation by glial cells. *Front. Aging Neurosci.* **8**, 160 (2016).
5. G. K. Gouras *et al*., Intraneuronal Abeta42 accumulation in human brain. *Am. J. Pathol.* **156**, 15–20 (2000).
6. F. M. LaFerla, K. N. Green, S. Oddo, Intracellular amyloid-beta in Alzheimer's disease. *Nat. Rev. Neurosci.* **8**, 499–509 (2007).
7. S. Oddo *et al*., Triple-transgenic model of Alzheimer's disease with plaques and tangles: Intracellular Abeta and synaptic dysfunction. *Neuron* **39**, 409–421 (2003).
8. H. Du *et al*., Cyclophilin D deficiency attenuates mitochondrial and neuronal perturbation and ameliorates learning and memory in Alzheimer's disease. *Nat. Med.* **14**, 1097–1105 (2008).
9. T. T. Olsson, O. Klementieva, G. K. Gouras, Prion-like seeding and nucleation of intracellular amyloid-β. *Neurobiol. Dis.* **113**, 1–10 (2018).
10. X. Hu *et al*., Amyloid seeds formed by cellular uptake, concentration, and aggregation of the amyloid-beta peptide. *Proc. Natl. Acad. Sci. U.S.A.* **106**, 20324–20329 (2009).
11. R. P. Friedrich *et al*., Mechanism of amyloid plaque formation suggests an intracellular basis of Abeta pathogenicity. *Proc. Natl. Acad. Sci. U.S.A.* **107**, 1942–1947 (2010).
12. M. Serra-Batiste *et al*., Aβ42 assembles into specific β-barrel pore-forming oligomers in membrane-mimicking environments. *Proc. Natl. Acad. Sci. U.S.A.* **113**, 10866–10871 (2016).
13. E. Wesén, G. D. M. Jeffries, M. Matson Dzebo, E. K. Esbjörner, Endocytic uptake of monomeric amyloid-β peptides is clathrin- and dynamin-independent and results in selective accumulation of Aβ(1-42) compared to Aβ(1-40). *Sci. Rep.* **7**, 2021 (2017).
14. H. H. Jarosz-Griffiths, E. Noble, J. V. Rushworth, N. M. Hooper, Amyloid-β receptors: The good, the bad, and the prion protein. *J. Biol. Chem.* **291**, 3174–3183 (2016).
15. R. G. Nagele, M. R. D'Andrea, W. J. Anderson, H. Y. Wang, Intracellular accumulation of beta-amyloid(1-42) in neurons is facilitated by the alpha 7 nicotinic acetylcholine receptor in Alzheimer's disease. *Neuroscience* **110**, 199–211 (2002).
16. J. V. Rushworth, H. H. Griffiths, N. T. Watt, N. M. Hooper, Prion protein-mediated toxicity of amyloid-β oligomers requires lipid rafts and the transmembrane LRP1. *J. Biol. Chem.* **288**, 8935–8951 (2013).
17. C. V. Zerbinatti *et al*., Apolipoprotein E and low density lipoprotein receptor-related protein facilitate intraneuronal Abeta42 accumulation in amyloid model mice. *J. Biol. Chem.* **281**, 36180–36186 (2006).
18. R. Limbocker *et al*., Trodusquemine enhances $A\beta_{42}$ aggregation but suppresses its toxicity by displacing oligomers from cell membranes. *Nat. Commun.* **10**, 225 (2019).
19. Q. Cao *et al*., Inhibiting amyloid-β cytotoxicity through its interaction with the cell surface receptor LilrB2 by structure-based design. *Nat. Chem.* **10**, 1213–1221 (2018).
20. P. P. Liu, Y. Xie, X. Y. Meng, J. S. Kang, History and progress of hypotheses and clinical trials for Alzheimer's disease. *Signal Transduct. Target. Ther.* **4**, 29 (2019).
21. L. Schneider, A resurrection of aducanumab for Alzheimer's disease. *Lancet Neurol.* **19**, 111–112 (2020).
22. J. Laurén, D. A. Gimbel, H. B. Nygaard, J. W. Gilbert, S. M. Strittmatter, Cellular prion protein mediates impairment of synaptic plasticity by amyloid-beta oligomers. *Nature* **457**, 1128–1132 (2009).
23. D. A. Gimbel *et al*., Memory impairment in transgenic Alzheimer mice requires cellular prion protein. *J. Neurosci.* **30**, 6367–6374 (2010).
24. F. Dohler *et al*., High molecular mass assemblies of amyloid-β oligomers bind prion protein in patients with Alzheimer's disease. *Brain* **137**, 873–886 (2014).
25. L. T. Haas *et al*., Metabotropic glutamate receptor 5 couples cellular prion protein to intracellular signalling in Alzheimer's disease. *Brain* **139**, 526–546 (2016).
26. J. W. Um *et al*., Metabotropic glutamate receptor 5 is a coreceptor for Alzheimer aβ oligomer bound to cellular prion protein. *Neuron* **79**, 887–902 (2013).
27. S. Dutta *et al*., Suppression of oligomer formation and formation of non-toxic fibrils upon addition of mirror-image Aβ42 to the natural l-enantiomer. *Angew. Chem. Int. Ed. Engl.* **56**, 11506–11510 (2017).
28. S. Dutta, T. S. Finn, A. J. Kuhn, B. Abrams, J. A. Raskatov, Chirality dependence of amyloid β cellular uptake and a new mechanistic perspective. *ChemBioChem* **20**, 1023–1026 (2019).
29. Z. Y. Wang *et al*., Knockdown of prion protein (PrP) by RNA interference weakens the protective activity of wild-type PrP against copper ion and antagonizes the cytotoxicity of fCJD-associated PrP mutants in cultured cells. *Int. J. Mol. Med.* **28**, 413–421 (2011).
30. D. C. Bode, M. D. Baker, J. H. Viles, Ion channel formation by amyloid-β42 oligomers but not amyloid-β40 in cellular membranes. *J. Biol. Chem.* **292**, 1404–1413 (2017).
31. M. A. Kostylev *et al*., Liquid and hydrogel phases of PrP(C) linked to conformation shifts and triggered by Alzheimer's amyloid-beta oligomers. *Mol. Cell* **72**, 426–443.e12 (2018).
32. D. Wade *et al*., All-D amino acid-containing channel-forming antibiotic peptides. *Proc. Natl. Acad. Sci. U.S.A.* **87**, 4761–4765 (1990).
33. S. T. Henriques, H. Peacock, A. H. Benfield, C. K. Wang, D. J. Craik, Is the mirror image a true reflection? Intrinsic membrane chirality modulates peptide binding. *J. Am. Chem. Soc.* **141**, 20460–20469 (2019).
34. J. P. Colletier *et al*., Molecular basis for amyloid-beta polymorphism. *Proc. Natl. Acad. Sci. U.S.A.* **108**, 16938–16943 (2011).
35. M. F. Knauer, B. Soreghan, D. Burdick, J. Kosmoski, C. G. Glabe, Intracellular accumulation and resistance to degradation of the Alzheimer amyloid A4/beta protein. *Proc. Natl. Acad. Sci. U.S.A.* **89**, 7437–7441 (1992).
36. I. R. Kleckner, M. P. Foster, An introduction to NMR-based approaches for measuring protein dynamics. *Biochim. Biophys. Acta* **1814**, 942–968 (2011).
37. N. D. Younan, K. F. Chen, R. S. Rose, D. C. Crowther, J. H. Viles, Prion protein stabilizes amyloid-β (Aβ) oligomers and enhances Aβ neurotoxicity in a *Drosophila* model of Alzheimer's disease. *J. Biol. Chem.* **293**, 13090–13099 (2018).
38. B. R. Fluharty *et al*., An N-terminal fragment of the prion protein binds to amyloid-β oligomers and inhibits their neurotoxicity in vivo. *J. Biol. Chem.* **288**, 7857–7866 (2013).
39. A. H. Brody, S. M. Strittmatter, Synaptotoxic signaling by amyloid beta oligomers in Alzheimer's disease through prion protein and mGluR5. *Adv. Pharmacol.* **82**, 293–323 (2018).
40. A. Aguzzi, C. Sigurdson, M. Heikenwaelder, Molecular mechanisms of prion pathogenesis. *Annu. Rev. Pathol.* **3**, 11–40 (2008).

41. P. Madhu, S. Mukhopadhyay, Preferential recruitment of conformationally distinct amyloid-β oligomers by the intrinsically disordered region of the human prion protein. *ACS Chem. Neurosci.* **11**, 86–98 (2020).
42. D. B. Freir *et al*., Interaction between prion protein and toxic amyloid β assemblies can be therapeutically targeted at multiple sites. *Nat. Commun.* **2**, 336 (2011).
43. C. Balducci *et al*., Synthetic amyloid-beta oligomers impair long-term memory independently of cellular prion protein. *Proc. Natl. Acad. Sci. U.S.A.* **107**, 2295–2300 (2010).
44. I. J. Whitehouse *et al*., Ablation of prion protein in wild type human amyloid precursor protein (APP) transgenic mice does not alter the proteolysis of APP, levels of amyloid-β or pathologic phenotype. *PLoS One* **11**, e0159119 (2016).
45. T. Kim *et al*., Human LilrB2 is a β-amyloid receptor and its murine homolog PirB regulates synaptic plasticity in an Alzheimer's model. *Science* **341**, 1399–1404 (2013).
46. M. Cissé *et al*., Ablation of cellular prion protein does not ameliorate abnormal neural network activity or cognitive dysfunction in the J20 line of human amyloid precursor protein transgenic mice. *J. Neurosci.* **31**, 10427–10431 (2011).
47. X. D. Shi *et al*., Blocking the interaction between EphB2 and ADDLs by a small peptide rescues impaired synaptic plasticity and memory deficits in a mouse model of Alzheimer's disease. *J. Neurosci.* **36**, 11959–11973 (2016).
48. E. Terzi, G. Hölzemann, J. Seelig, Interaction of Alzheimer beta-amyloid peptide(1-40) with lipid membranes. *Biochemistry* **36**, 14845–14852 (1997).
49. J. Habchi *et al*., Cholesterol catalyses Aβ42 aggregation through a heterogeneous nucleation pathway in the presence of lipid membranes. *Nat. Chem.* **10**, 673–683 (2018).
50. S. Jin *et al*., Amyloid-β(1-42) aggregation initiates its cellular uptake and cytotoxicity. *J. Biol. Chem.* **291**, 19590–19606 (2016).
51. R. Freer *et al*., A protein homeostasis signature in healthy brains recapitulates tissue vulnerability to Alzheimer's disease. *Sci. Adv.* **2**, e1600947 (2016).
52. R. Kundra, P. Ciryam, R. I. Morimoto, C. M. Dobson, M. Vendruscolo, Protein homeostasis of a metastable subproteome associated with Alzheimer's disease. *Proc. Natl. Acad. Sci. U.S.A.* **114**, E5703–E5711 (2017).
53. T. Fülöp, R. F. Itzhaki, B. J. Balin, J. Miklossy, A. E. Barron, Role of microbes in the development of Alzheimer's disease: State of the art–An international symposium presented at the 2017 IAGG congress in San Francisco. *Front. Genet.* **9**, 362 (2018).
54. T. Fülöp *et al*., Targeting infectious agents as a therapeutic strategy in Alzheimer's disease. *CNS Drugs* **34**, 673–695 (2020).
55. G. Ill-Raga *et al*., Activation of PKR causes amyloid ß-peptide accumulation via derepression of BACE1 expression. *PLoS One* **6**, e21456 (2011).
56. D. M. Cairns *et al*., A 3D human brain-like tissue model of herpes-induced Alzheimer's disease. *Sci. Adv.* **6**, eaay8828 (2020).
57. G. P. Roseman, "The central region of the cellular prion protein attenuates the intrinsic toxicity of N-terminus," PhD thesis, University of California, Santa Cruz, CA (2019).
58. E. G. Evans, M. J. Pushie, K. A. Markham, H. W. Lee, G. L. Millhauser, Interaction between prion protein's copper-bound octarepeat domain and a charged C-terminal pocket suggests a mechanism for N-terminal regulation. *Structure* **24**, 1057–1067 (2016).
59. A. R. Spevacek *et al*., Zinc drives a tertiary fold in the prion protein with familial disease mutation sites at the interface. *Structure* **21**, 236–246 (2013).
60. F. Delaglio *et al*., NMRPipe: A multidimensional spectral processing system based on UNIX pipes. *J. Biomol. NMR* **6**, 277–293 (1995).